Modelling and analysis of the MSFR transient behaviour

Carlo Fiorina [a], Danny Lathouwers [b], Manuele Aufiero [a], Antonio Cammi [a], Claudia Guerrieri [a], Jan Leen Kloosterman [b], Lelio Luzzi [a,*], Marco Enrico Ricotti [a]

[a] *Politecnico di Milano, Department of Energy, Nuclear Engineering Division, via Ponzio 34/3, 20133 Milano, Italy*
[b] *Technical University of Delft, Department of Radiation Science & Technology, Mekelweg 15, 2629 JB, Delft, Netherlands*

Received 12 January 2013
Accepted 5 August 2013
Available online 5 September 2013

1. Introduction

Molten Salt Reactors (MSRs) were conceived during the fifties for military purposes in the US, and subsequently developed for two decades as graphite-moderated U-233 breeder reactors for power production (MacPherson, 1985). A renewed impetus has been given to the MSR R&D by the Generation IV International Forum (GIF-IV) that, in 2001, selected the MSR as one of the six innovative nuclear reactors with the potential to meet the compelling need for an increasingly sustainable, economical, safe and proliferation resistant nuclear energy production (GIF-IV, 2002). Few years after the selection of the MSR among the Generation-IV reactors, the concept evolved in the direction of fast-spectrum MSRs (MSFR – Molten Salt Fast Reactors). Adoption of a fast-neutron spectrum guarantees a better breeding and good capabilities for TRU (TRans-Uranic isotope) burning (Fiorina et al., 2013). It is noteworthy that the MSR requires extended definitions of the breeding gain to take into account the uranium in the external stock (Nagy et al., 2011, 2012). It is also expected to improve safety, as one of the historical problems of MSRs was the positive reactivity feedback coefficient of the graphite moderator (Renault et al., 2005). On the other hand, drawbacks exist like a higher actinide inventory and exacerbated material problems. More generally, a limited know-how is available for fast-spectrum MSR technology.

Among various aspects requiring investigation, the present paper focuses on the reactor dynamics and safety features. A first objective is benchmarking two different models developed at the *Politecnico di Milano* and at the *Technical University of Delft* for the transient analysis of the MSFR primary circuit. They include a coupled representation of thermal–hydraulics and neutronics. The governing partial differential equations are discretized and solved in a simplified 2-D $r-z$ geometry. The second objective is to use the results from code benchmarking to attain a first understanding of the MSFR transient behaviour, pointing out the most critical issues to be taken into account during reactor design and optimization.

In Section 2, the investigated reactor concept is presented. Section 3 discusses the adopted methodology. After a preliminary assessment of the MSFR neutronic features (Section 4), the MSFR steady-state and transient behaviour are discussed in Sections 5 and 6, respectively. The conclusions of the work are finally drawn in Section 7.

* Corresponding author. Tel.: +39 02 2399 6326.
E-mail address: lelio.luzzi@polimi.it (L. Luzzi).

Nomenclature

Latin symbols

D_i	decay heat of the ith group (W/m^3)
f_i	fraction of power generation associated to the ith decay heat group (–)
Q	internal heat generation in the fuel salt (W/m^3)
r	radial coordinate (m)
t	time (s)
T	temperature (K)
T_0	reference temperature (K)
$\boldsymbol{u}$	velocity vector (m/s)
z	axial coordinate (m)

Greek symbols

α_ρ	feedback coefficient for fuel expansion (pcm/K)
β	fuel expansion coefficient (K^{-1})
β_{eff}	effective delayed neutron fraction (pcm)
λ_i	decay constant associated to the ith decay heat group (s^{-1})
μ_T	turbulent viscosity (Pa s)
ρ_S	fuel salt density (kg/m^3)

2. Investigated reactor concept

The MSFR is analysed in the present paper. It is the reference circulating-fuel MSR in the framework of the Generation IV International Forum, and it is mainly developed in the EURATOM EVOL Project (EVOL, 2013). The core of the MSFR is a cylinder with a diameter equal to the height, surrounded axially by 1-m thick steel reflectors, and radially by a fertile blanket, a boron carbide layer, and a reflector. The main core parameters are summarized in Table 1, while a schematic view is reported in Fig. 1.

The fuel salt is composed of LiF for 77.5 mol%, and a mixture of AcF_3 and AcF_4 for 22.5% (Ac indicates actinides). For the specific computations performed in this paper, a beginning-of-life ^{232}Th–^{233}U (88.69–11.31 wt.%) fuel salt composition is assumed (Merle-Lucotte et al., 2011).

The MSFR envisions the use of an intermediate circuit to separate the radioactive primary coolant from the energy conversion system. The intermediate circuit uses molten FLiNaK (Benes and Konings, 2009) as coolant. The heat transfer between primary and intermediate circuits is achieved through 16 heat exchangers, whose exact design has not yet been defined. In this paper, a shell-and-tube configuration will be considered, with the primary salt in the tubes and the secondary salt in the shell. This is consistent with the MSRE (Molten Salt Reactor Experiment) and MSBR (Molten Salt Breeder Reactor) designs developed at the Oak Ridge National Laboratory during the Molten Salt Reactor Project (Robertson, 1971; Energy from Thorium website). The shell has been configured to achieve the same heat transfer coefficient as for the primary salt. At the secondary side, a constant temperature of 823 K has been assumed. The following main constraints specified for the MSFR, and mainly characterizing the core transient behaviour, have been taken into account: (1) inlet/outlet temperatures equal to 923/1023 K, respectively and (2) a total volume on the primary side equal to 36% of the salt in the external part of the primary circuits (i.e., in pipes, pumps and heat exchangers). Results of the preliminary design process are reported in Table 2, though it is worth pointing out that technical or economic constraints may lead to different designs, with potentially notable impacts e.g. on the pressure losses.

Table 1
MSFR core parameters (Merle-Lucotte et al., 2011).

Thermal/electric power	3000 MW$_{th}$/1500 MW$_e$
Core inlet/outlet temperatures	923/1023 K
Fuel salt volume	18 m^3
Fraction of salt inside the core	0.5
Blanket thickness	50 cm
Blanket salt volume	7.3 m^3
Boron carbide layer thickness	20 cm
Salt density	$(4094–8.82 \times 10^{-1}\cdot(T[\text{K}]\text{-}1008))$ kg/m^3
Salt specific heat	$-1111 + 2.78\ T$ [K] J/kg K
Salt thermal conductivity	$0.928 + 8.397 \times 10^{-5}\ T$[K] W/m K
Salt kinematic viscosity	5.54×10^{-8} exp $(3689/T[\text{K}])$ m^2/s
Flow rate	4.5 m^3/s

3. Modelling approach

This section presents the models developed at the *Politecnico di Milano* (from here on referred to as Polimi) and at the *Technical University of Delft* (from here on referred to as TUDelft) for the transient analysis of the MSFR. Modelling choices are mostly consistent for the two models and differences will be explained when relevant.

3.1. Geometry and main assumptions

The current MSFR conceptual design features a nearly axial-symmetric core geometry, which allows for a 2D modelling. The axial-symmetric representation can be extended to the entire primary circuit by approximating the 16 external loops with a single annular loop (Fig. 2), provided that detailed velocity and temperature distributions in the external part of the circuit are not of interest. Ensuing drawbacks are mainly: (1) approximate pressure drops and mixing effects in the out-of-core part of the circuit; (2) the impossibility to predict some local effects in the core, like the flow pattern close to inlet and outlet of each loop; (3) the impossibility to explicitly represent pump and heat exchanger. The latter shortcoming can be partly overcome by substituting pump and heat exchanger with suitable momentum and heat sources (or sinks).

The heat exchanger was simulated by a volume force opposite to the fluid flow and causing an overall pressure drop of 300 kPa (Table 2) at nominal conditions. To take into account the velocity-dependency of the pressure losses and in view of the turbulent flow in the tubes, the volume force has been multiplied by the ratio between actual and nominal flow rates, to the power of 1.75 (Incropera et al., 2006). The pump was simulated by a volume force in the direction of the flow and able to establish the nominal volumetric flow rate of 4.5 m^3/s.

The heat transfer with the intermediate circuit has been simulated through a heat sink proportional to the temperature difference between primary and secondary circuits, and to the harmonic mean of the heat transfer coefficients on each side of the heat exchanger. The heat transfer coefficient related to the primary circuit has been provided with a dependency on velocity in accordance with the Dittus–Boelter correlation (Dittus and Boelter, 1930). Volume and position occupied by the heat sink are in this case important for a proper transient simulation. The occupied

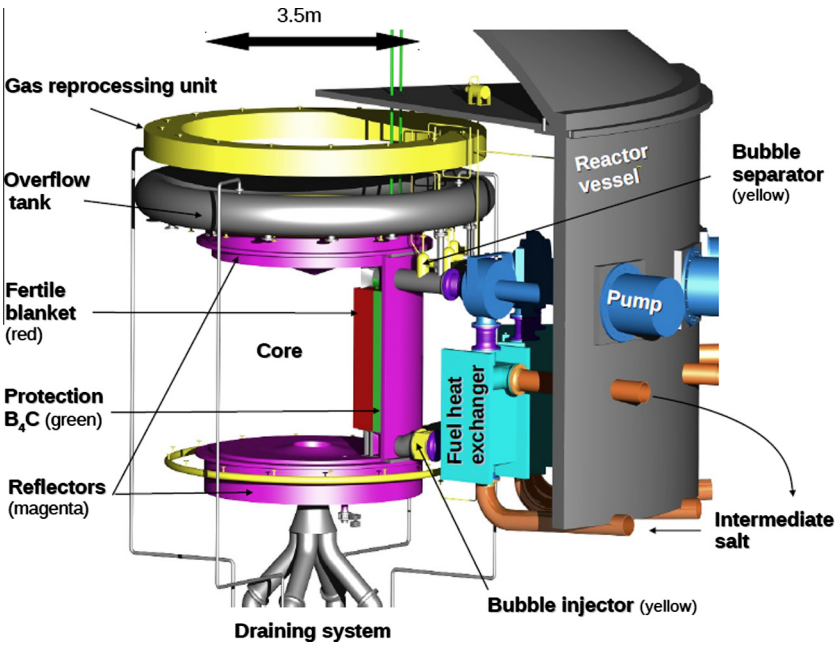

Fig. 1. Schematic view of the MSFR primary circuit: the fuel circulates through the core and 16 external circuits, each one including a pump and a heat exchanger; an overflow tank accommodates salt expansion in case of overheating; the entire primary circuit is contained in a secondary reactor vessel (Brovchenko et al., 2012).

Table 2
Heat exchanger parameters.

Type	Tube (primary circuit) and shell (secondary circuit)
Power exchange	187.5 MW
Inlet/outlet temperatures (primary side)	1023/923 K
Fuel salt volume (primary side)	0.203 m^3
Tube inner diameter	0.4 cm
Tube length	2 m
Number of tubes	8061
Temperature of the secondary side	823 K
Heat transfer coefficient on each side of the heat exchanger	2.60×10^6 W/K
Salt velocity (primary side)	2.78 m/s
Reynolds number (primary side)	4600
Pressure loss (primary side)	300 kPa

volume has been set to 36% of the out-of-core part of the primary circuit, consistently with the preliminary design reported in Table 2. The heat source has been placed in the upper part of the out-of-core circuit (see Fig. 2) to enable natural circulation in case of a loss of flow.

It is also worth mentioning that the use of an axial-symmetric flow model excludes possible non-symmetric flow patterns, which are in principle allowed by the non-linearity of the Navier–Stokes equations. However, use of an axial-symmetric model drastically reduces the computational requirements, without substantially jeopardizing the capability of the model to investigate the overall system behaviour. Also, apart from the apparent savings in computational cost, the high-Reynolds two-equation models used in the present work are likely to result in symmetric solutions even for full 3D studies due to their diffusive behaviour compared to low-Reynolds number models. This further supports our choice of using an axisymmetric geometry.

3.2. Multi-physics modelling

To simulate the MSFR steady-state and transient behaviour, a multi-physics approach has been adopted envisioning a node-wise coupling of the various quantities. Specifically, the models employed in this paper couples thermal–hydraulics, neutronics and delayed neutron precursor movement.

Thermal–hydraulics is modelled through Reynolds-Averaged Navier–Stokes (RANS) equations for mass conservation, momentum conservation in the axial direction and momentum conservation in radial direction. The compressible form of these equations is assumed for the Polimi model, while an incompressible flow is assumed for the TUDelft model, with natural circulation effects taken into account through the Boussinesq approximation. The local turbulent viscosity is obtained by solving the standard $k-\varepsilon$ model with logarithmic wall functions.

Temperature distributions are obtained by means of a classical equation for energy conservation, with the turbulent conductivity that is derived from the turbulent viscosity, assuming a turbulent Prandtl number equal to 0.85. A condition of thermal insulation is applied at the external boundaries of the geometry and around the blanket, where the temperature field is not solved. In the TUDelft model instead, conditions of thermal insulation are applied to all boundaries between fuel salt and core structures, and the temperature field is solved only in the salt.

Neutron fluxes are represented according to a multi-group diffusion approach explicitly adapted for precursor movement (see, e.g., Kophazi et al., 2009; Cammi et al., 2011, 2012; Van der Linden, 2012). Six energy groups are used for the Polimi model and the cross-sections are derived for each material using the SERPENT Monte Carlo code (Leppänen, 2007) and the JEFF-3.1 library (Koning et al., 2006). A simple logarithmic temperature dependence is employed, using the cross-sections at 900 K and 1200 K for the interpolation. Cross-sections are also assumed to be directly proportional to the local density. Nine energy groups are instead used in the TUDelft model, with the cross-sections derived from the deterministic code SCALE (SCALE, 2006) and the ENDF/B-VII.0 library (Chadwick et al., 2006). Cross-sections are computed every 100 K and a square-root interpolation is performed between these points. In this case, density dependency is included in the temperature dependency. Different cross-section sets are used based both on the material and on the position in the core. In particular, for a given material, a cross-section set is computed for different radial

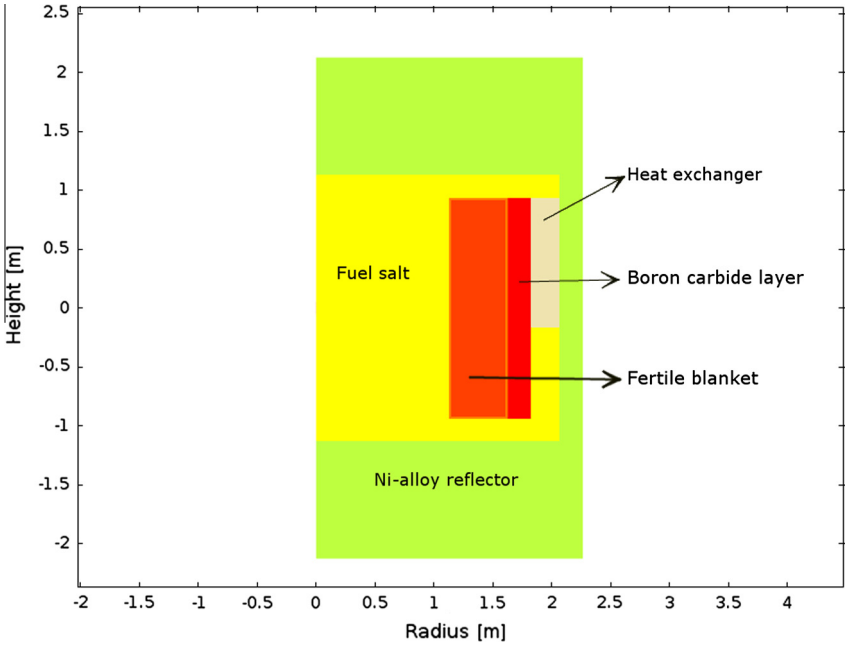

Fig. 2. Schematic view of the investigated geometry: the primary circuit is approximated as a annular loop to allow for a 2D representation.

and axial positions, the subdivision being based on the spatial discretization used for the neutronic calculations (see van der Linden (2012) for further details).

In both the Polimi and TUDelft models, the fraction of delayed neutrons that are generated in an energy group is calculated using SERPENT or SCALE and directly used in the multi-physics model as a source term for the corresponding precursor equations. This is an approximation when using a broad energy structure, since it does not allow to properly take into account the effectiveness of the delayed neutrons. However, the approximation was found to be relatively small (few per cents, see e.g. Fiorina et al., 2012, 2013) and can be considered acceptable for the purposes of this paper, which aims at a general characterization of the MSFR dynamics. In case of MSRs, the movement of the delayed neutron precursors affects differently the effectiveness of delayed neutrons in each precursor group. An accurate calculation of the different effective delayed neutron fractions in circulating fuel conditions is beyond the scope of the present work and is the subject of current studies of some of the authors.

Eight and six precursor groups are employed in the Polimi and TUDelft models, respectively, with the time constants inherited from the respective nuclear data libraries. To take into account the fuel salt motion, a convective term is included in the precursor equations (see, e.g., Kophazi et al., 2009, Cammi et al., 2011, 2012, Van der Linden, 2012), with a turbulent diffusivity computed from the turbulent viscosity and assuming a turbulent Schmidt number equal to 0.85.

The boundary conditions for the equations describing neutron diffusion, and precursor diffusion and convection are the same for the Polimi and TUDelft codes. In particular, a zero-neutron-flux boundary condition is applied to the external boundaries of the geometry while homogeneous Neumann conditions are applied to the precursor equations at the boundaries of the fuel salt domain.

Finally, the Polimi model includes three equations to simulate the behaviour of the isotopes responsible for the decay heat. In particular, the following equation form is employed:

$$\frac{dD_i}{dt} + \nabla \cdot \frac{\mu_T}{\rho_s 0.85} \nabla D_i + \boldsymbol{u} \cdot \nabla D_i + \lambda_i D_i = Q f_i \lambda_i \quad \text{for} i = 1,2,3 \qquad (1)$$

λ_i and f_i have been derived through interpolation of the decay heat after reactor shutdown provided by SERPENT. Their values are listed in Table 3.

3.3. Discretization and numerical solution

A finite element discretization scheme with Lagrangian linear elements is adopted in the Polimi model. The mesh is triangular, with a progressive refinement close to the walls between salt and core structures. In the vicinity of the walls, rectangular elements are used. Fig. 3 shows the adopted mesh in the vicinity of the core inlet. The total number of cells is equal to 39,896, resulting in 237,490 degrees of freedom. The equations are discretized and solved using the commercial software COMSOL Multiphysics (Comsol, 2011).

The TUDelft model is based on the coupling between two in-house developed codes. Specifically, the DALTON code (see e.g., Boer et al. (2010)) is used for neutron transport and precursor diffusion and convection. This code has also the capability for adjoint eigenvalue calculations. The finite-volume code HEAT (De Zwaan et al., 2007) is used for the CFD analysis. In addition, cross-section interpolation is performed using dedicated SCALE sub-procedures. The overall coupling is achieved through a PERL script. DALTON and HEAT adopt two different rectangular meshes and a Fortran routine performs projections from one mesh to the other. A coarser mesh (Fig. 4) is used for DALTON, resulting in 5148 elements. The mesh adopted for HEAT has been achieved using 16 cells for each cell used in DALTON. Further details about the TUDelft model can be found in De Zwaan et al. (2007) and Van der Linden (2012).

Table 3
Parameters adopted to model decay heat. λ_i and f_i are the decay constants and power fractions associated to the decay heat groups.

Decay heat group	λ_i (s^{-1})	f_i (–)
1	0.1974	0.0117
2	0.0168	0.0129
3	3.58×10^{-4}	0.0186

4. Preliminary neutronic assessment

Before discussing the detailed results of the multi-physics modelling, this section describes preliminary assessment studies dedicated at a comparison between the results provided by Polimi and TUDelft models for the sole neutronics. In fact, the capability of the two models to reproduce reactivity feedbacks, generation time and effective delayed neutron fraction (β_{eff}) is essential for providing consistent results in terms of steady state and, particularly, transient reactor behaviour. A detailed neutronic assessment of the Polimi model can be found in Fiorina et al. (2012) and (2013), where it has been proved able to predict with good accuracy the MSFR neutronic features, for different fuel compositions. The TUDelft code used for neutronics has been extensively benchmarked earlier, for example for PBMR studies (Boer et al., 2010) and for other molten salt related investigations (Kophazi et al., 2009).

The capability of the Polimi and TUDelft models to predict the β_{eff} has been tested adopting static and iso-thermal (973 K) salt conditions, so as to avoid influences on results related to different velocity and temperature fields. The Polimi model is not capable of adjoint flux calculations and computation of the β_{eff} cannot be directly performed. However, the β_{eff} can be estimated as a difference between reactivities computed through two λ-eigenvalue computations with and without precursor source. For the sake of consistency, this method has been used for both codes. As a result, 299.8 pcm and 289.4 pcm are predicted by the Polimi and TUDelft models, respectively, showing an acceptable 3% discrepancy. An α-eigenvalue computation can be used to approximate the neutron generation time (Lathouwers, 2003; Singh et al., 2009). The Polimi model predicts a generation time equal to 1.03 μs, to be compared to the 0.91 μs of the TUDelft model. In this case, the discrepancy between the two models is of the order of 10–15%, which has been ascribed to the different nuclear data libraries employed to compute the cross-sections.

The salt temperature affects reactivities directly through the Doppler effect and indirectly through density variation. Both effects give a negative feedback, which is typically of the same order of magnitude at the MSFR operating conditions (Fiorina et al., 2012). However, Doppler effect decreases logarithmically with energy (Fiorina et al., 2012), while, according to a 6-factor formula for reactivity, the density coefficient is expected to grow with increasing temperature roughly as:

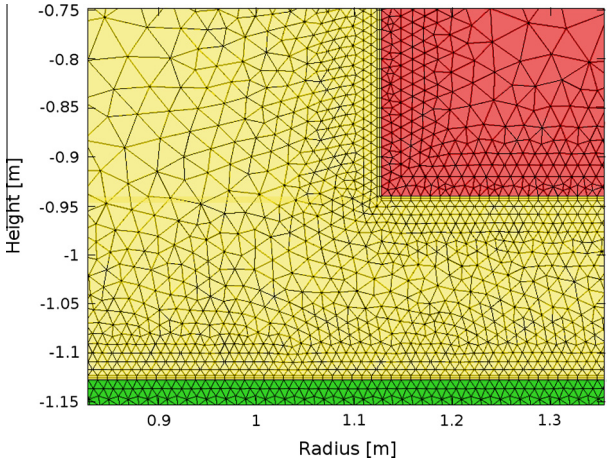

Fig. 3. Mesh adopted by the Polimi model in the vicinity of the core inlet.

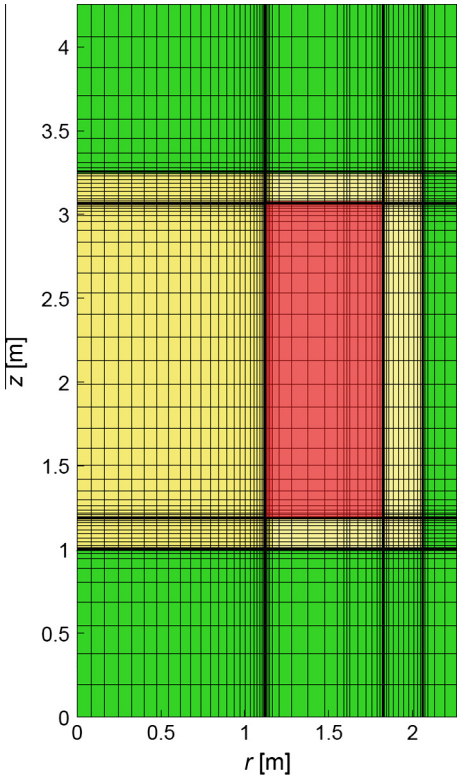

Fig. 4. Mesh adopted for solving neutron fluxes and precursor distributions in the TUDelft model.

$$\alpha_\rho(T) \propto \frac{1}{(1-\beta(T-T_0))^2} \tag{2}$$

According to these predictions, Fig. 5 shows that the overall reactivity feedback coefficient (computed for an isothermal reactor) features a minimum at approximately 1300 K. This implies that at the temperatures of interest for the MSFR, and for the given fuel salt composition, the Doppler effect is dominant. The agreement between Polimi and TUDelft models is excellent for the temperature range of interest for the MSFR, namely between salt freezing (838 K) and melting of the nickel alloy for the core structures (approximately 1600 K). The jigsaw behaviour of the coefficient predicted by TUDelft is to be ascribed to cross-section preparation with SCALE. As usual in core physics codes, SCALE adopts cross-section libraries prepared (e.g., using NJOY) at selected temperatures (typically, 600 K, 900 K, 1200 K, etc.) and performs interpolation to predict cross-sections in-between. Hence, it is expected to give "exact" solutions only at the temperatures where cross-sections are directly available. As a confirmation, it can be observed that Polimi and TUDelft models predict nearly the same coefficient at 600 K, 900 K and 1200 K. The smooth trend of the coefficient predicted by the Polimi model is related to the fact that only two cross-section sets (at 900 K and 1200 K) have been used for the interpolation. A non-negligible discrepancy can be observed between the two models above 1500 K. At these temperatures, the feedback coefficient is dominated by density effects, and the cross-sections of the TUDelft model were computed using a slightly lower fuel expansion coefficient ($1.78{\cdot}10^{-4}$ K^{-1} instead of $2.15{\cdot}10^{-4}$ K^{-1}, consistently with previously available data). However, impact on the results presented in this paper is negligible since temperatures above 1500 K are generally not reached.

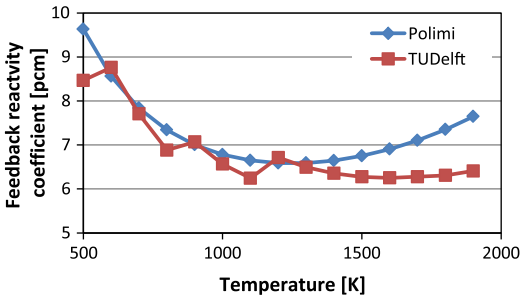

Fig. 5. Temperature dependency of the salt temperature reactivity feedback coefficient.

5. Steady-state reactor behaviour

5.1. Thermal–hydraulics

Fig. 6 shows the temperature and velocity fields in the core of the MSFR as predicted by the Polimi and TUDelft models. For a better comparison, decay heat from actinides and fission products has been turned off in the Polimi model, even though its impact is small. The velocity field is predicted consistently by the two models. In particular, a wide recirculation zone exists close to the blankets, while the fuel is nearly stagnating at the core centre, close to the axial reflectors. Recirculation is due to inertial and viscous effects, while removal of the gravity force does not impact significantly the results.

Recirculation leads to temperatures inside the core active region well above the outlet ones. In the recirculation zone close to the blankets, the predicted temperature is approximately 200 K higher than at the outlet. Although acceptable in terms of melting temperature of the core structures (~1500–1600 K), this generates unnecessary thermal stress and material problems that could be avoided through an improved thermal–hydraulic design. R&D efforts in this direction are already being spent in the framework of the EURATOM EVOL Project (EVOL, 2013) and include investigations of: (1) suitable diffusors at the core inlet; (2) use of a distribution plate at the bottom of the core; and (3) hourglass shaping of the active core region.

The Polimi model generally predicts higher local temperatures in the recirculation zones, which is related to a lower predicted turbulent viscosity (and turbulent conductivity), as shown in Fig. 7. Turbulent viscosity depends on turbulent kinetic energy and dissipation, which in turn are predicted by the $k-\varepsilon$ turbulence model. Differences can partly be ascribed to different meshes. In particular, a full mesh independence of the solution was not obtained in the TUDelft model due to the excessive computational requirements. In addition, some coding details differ between the two models, like for instance the numerical method for the solution and the implementation of wall functions.

In order to have an indication on the uncertainties related to the thermal–hydraulic calculation, a different turbulence modelling has also been employed. Specifically, an additional calculation has been performed with the Polimi model substituting the $k-\varepsilon$ with the $k-\omega$ (Wilcox, 1998) turbulence model. Wider recirculation zones have been observed, including a stagnation zone at the radial axis, close to the upper reflector. Predicted temperatures in the recirculation zone close to the blanket are tens of degrees higher than those predicted by the $k-\varepsilon$ model and they reach 1500 K in the mentioned stagnation point. This confirms for the MSFR case the well-known difficulties of the two-equation RANS turbulence models in predicting recirculation and stagnation phenomena.

5.2. Neutronics

Neutron fluxes are not affected by fuel-salt motion and maintain the typical symmetric shape generally observed in nuclear reactors. Polimi and TUDelft predictions are not reported here for brevity but details can be found in Fiorina et al. (2012) and van der Linden (2012). Distribution of precursors and, consequently, of the delayed neutron source is instead of interest as it is a unique feature of the MSFR. In addition, it is strongly coupled to the thermal–hydraulics of the core and differences are expected between the two models following the differences in the predicted turbulent viscosity. Fig. 8a and b plot the delayed neutron source as predicted by the Polimi and TUDelft model, respectively. It appears clearly how delayed neutrons are emitted throughout the primary circuits, with a detrimental effect on β_{eff}. In particular, roughly 65% of delayed neutrons are emitted inside the core, while the others are emitted in the out-of-core path of the salt and do not contribute to β_{eff}. The effectiveness of delayed neutrons is further reduced by the axial drift of the salt, which brings precursors outside of the high-flux region at the core centre. As a result, the β_{eff} at the MSFR operating conditions results equal to 134.3 pcm and 123.8 pcm for the Polimi and TUDelft models, respectively. The ~10 pcm discrepancy in the β_{eff} is consistent with the difference in the β_{eff} for static fuel (299.8 pcm and 289.4 pcm).

Agreement between the two codes in terms of precursor distribution is good. In particular, the fraction of precursors that decays in the out-of-core part of the primary circuit amounts to 34.80% and 34.85% in the Polimi and TUDelft models, respectively. Consistently with the lower turbulent diffusivity pointed out in the previous subsection, the high-delayed-neutron-source regions close to the axial reflectors are wider in the Polimi model. On the other hand, the predicted delayed neutron source in the large recirculation area close to the blanket is higher in the TUDelft model, which can be ascribed to the different delayed neutron groups adopted for the two models. The reduction of β_{eff} is equal to 55% and 57% in the Polimi and TUDelft model, respectively.

6. Transient behaviour

Similarly to most reactor concepts, three main transient initiators can be identified for the MSFR, resulting in 5 main accidental transients. A reactivity insertion is the first relevant initiator and results in an accidental transient if a positive reactivity is inserted. In the MSFR, control rods may not be necessary to balance the reactivity swing thanks to the on-line reprocessing system, but they may be necessary to drive the reactor operational transients (start-up, shut-down, load following). In addition, malfunctioning of the reprocessing system may cause in principle a quick injection of fissile material. The primary pumps represent a second transient initiator. They may trigger different accidental transients as they may experience an overspeed or a coast-down. Finally, the heat exchangers may lose or increase their cooling capabilities following abnormal events in the intermediate or secondary circuits.

The following subsections discuss the MSFR response to the mentioned transient initiators. In view of the axial-symmetry of the developed models, only symmetric transients will be investigated, while it is not possible to deal e.g. with abnormal events occurring to one or few of the 16 primary loops.

The effect of decay heat has been found to be negligible in case of reactivity and pump driven transients (Sections 6.1–6.3), as well as in case of enhanced cooling at the heat exchangers (Section 6.4). For this reason, the equations simulating the decay heat in the Polimi model will not be used in these cases, that allows for a

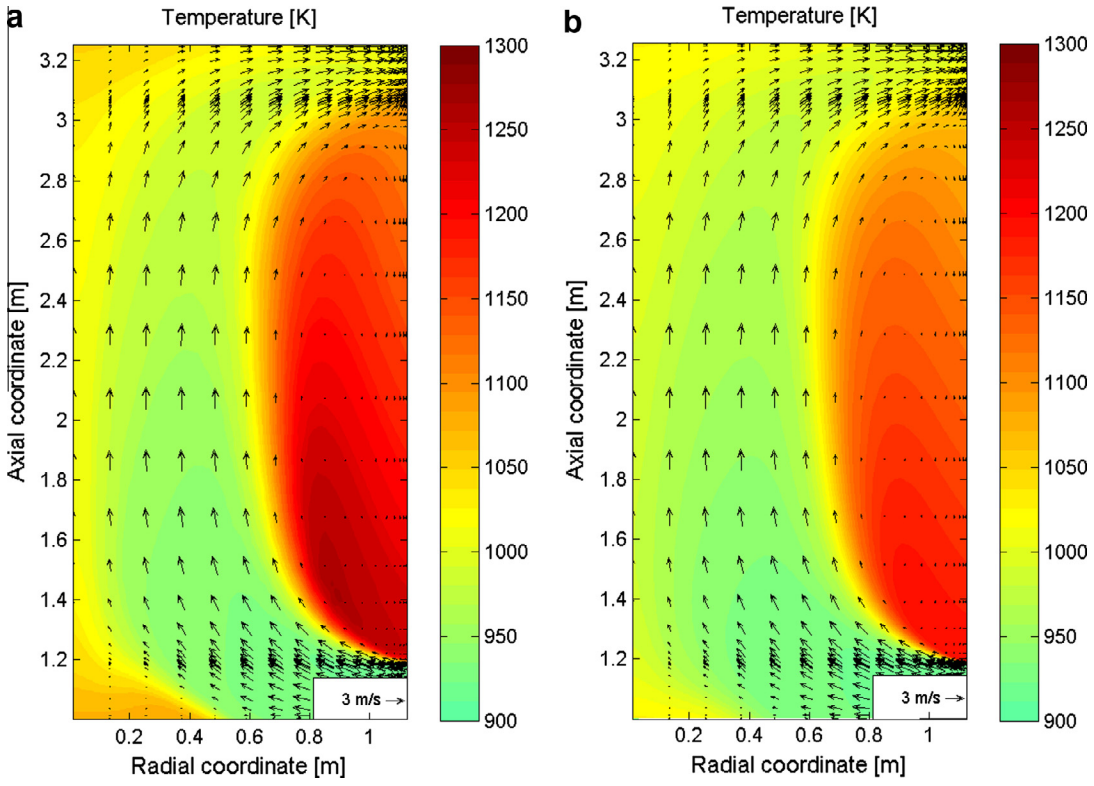

Fig. 6. Velocity and temperature fields in the core predicted by (a) Polimi model and (b) TUDelft model.

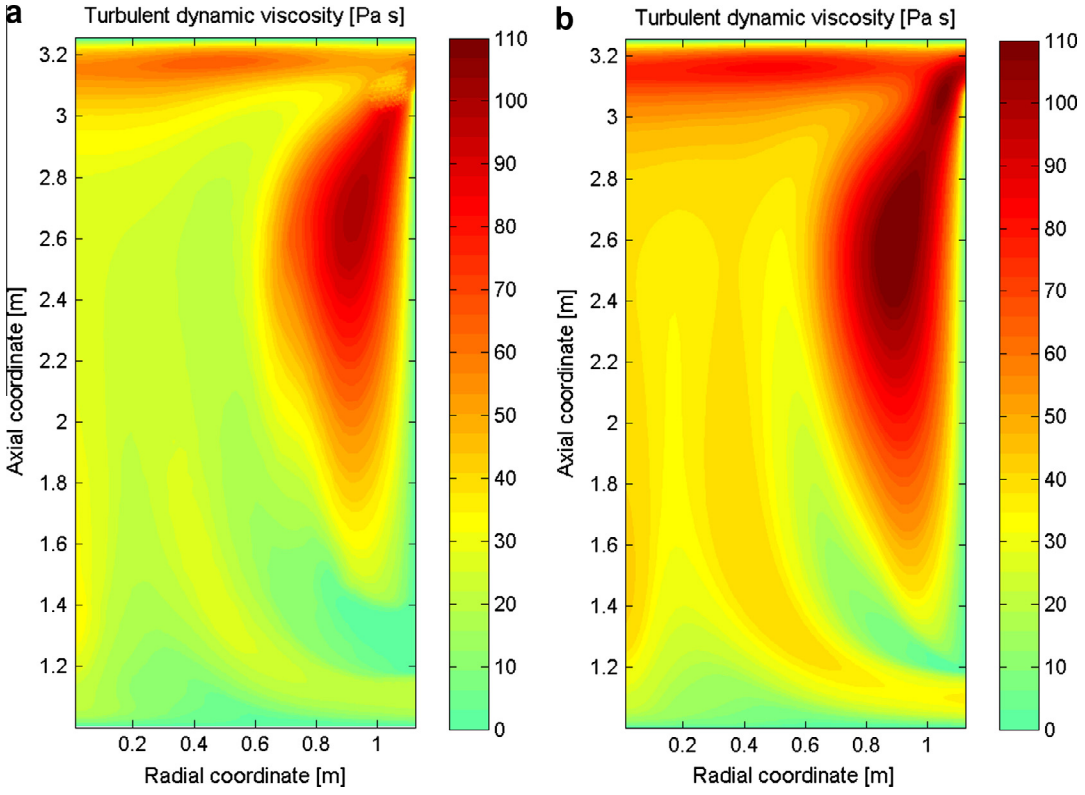

Fig. 7. Turbulent dynamic viscosity in the core predicted by (a) Polimi model and (b) TUDelft model.

better comparison with the TUDelft model. The effect of decay heat will instead be included in Section 6.5, which discusses the system response to a loss of heat sink.

As a general comment, presented results are not intended as a comprehensive safety analysis, which would require a detailed core design (probably without recirculation zones). In addition, a

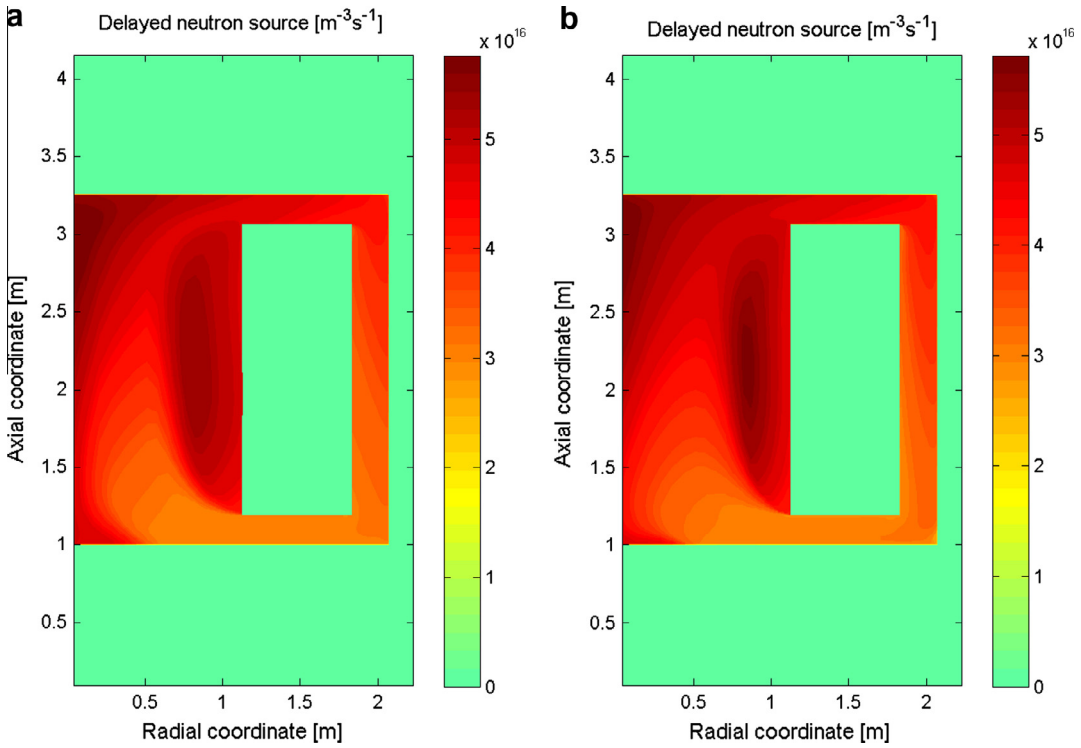

Fig. 8. Delayed neutron source in the primary circuit predicted by (a) Polimi model and (b) TUDelft model.

proper safety analysis would require details about the system design, which are currently unavailable. For instance, the reactor behaviour during a loss of flow is strongly dependent on the pressure drop in the circuit, its variation with the velocity field, and the variation of the heat transfer coefficient at the primary side of the heat exchanger. The pressure drop strongly depends on the heat exchanger design, which is still speculative at the current stage of development. Localized pressure drops at the heat exchanger inlet and outlet, and in the pump, should also be taken into account. In addition, the velocity dependence of pressure drop and heat transfer coefficient should be carefully evaluated, while here simple dependencies have been used assuming turbulent and fully developed hydrodynamic conditions. Hence, presented results aim mainly at: (1) benchmarking the two models developed in view of their future application e.g. to future MSFR designs or other MSR concepts; (2) pointing out the most critical issues to be taken into account while designing and optimizing fast-spectrum MSRs; and (3) giving general indications about the MSFR transient behaviour.

6.1. Unprotected transient over power – UTOP

A definite design is not available for the MSFR control or reprocessing system, so it is not yet possible to define worst-case scenarios for the transient overpower. For simplicity, two step-wise reactivity insertions have been investigated, namely: a 50 pcm insertion and a super-prompt-critical 200 pcm insertion. A step-wise insertion is particularly demanding from a numerical viewpoint, thus representing a good test for the models. In addition, it gives rise to the maximum power excursion for a given reactivity insertion. Fig. 9 shows the evolution of power and average core temperature for the two reactivity insertions.

The initial power increase triggered by the reactivity insertion is counteracted by Doppler effect and salt expansion. The power decreases and, for a few seconds, it tends to stabilize. After 2–3 s, the salt heated up during the initial power peak re-enters the core, causing a sudden power decrease. Power and core temperatures then stabilize at a new level without additional oscillations. The final core temperature increase is set by the amplitude of the reactivity step. In fact, the final reactivity reduction due to the salt temperature increase must balance exactly the initial reactivity insertion. In this sense, it is worth noting that the ratio between the final average core temperature increase and the initial reactivity insertion is equal 6 pcm/K, i.e., ∼10% lower compared to the coefficients predicted in Fig. 5 using isothermal reactor conditions. This is mainly related to the fact that an "effective" core temperature should be used to calculate reactivity feedbacks. The predicted coefficient becomes 6.9 pcm/K if direct and adjoint fluxes provided by DALTON are used as weight for the temperature distribution.

The energy released during the initial power peak is limited and deposits directly into the coolant, so that no core damage is expected even in the unrealistic scenario of a step-wise reactivity insertion. In addition, the core final temperature rise is limited by the strong temperature reactivity feedback even in the case of a super-prompt-critical reactivity insertion (which would probably be excluded by design). The limited impact of a reactivity insertion combines with the lack of a burn-up reactivity swing (and of the control rods necessary to counterbalance it) and with the atmospheric operating pressure to make a control rod extraction a lower concern in the MSFR. This is not the case e.g. for classical liquid–metal fast reactors, where reactivity swing can be notable (especially in TRU-burner concepts) and consequences of an UTOP pose strict constraints on control rod worth and, consequently, on the minimum number of necessary control rods (Wade et al., 1997). In addition, it is worth noting that reactivity insertion from the reprocessing system is a much lower concern in the MSFR compared to other MSRs. In fact, thanks to the fast spectrum, the reprocessing requirements are generally on the order of few litres or few tens of litres per day, which allows to strongly limit the maximum fuel insertion rate by design.

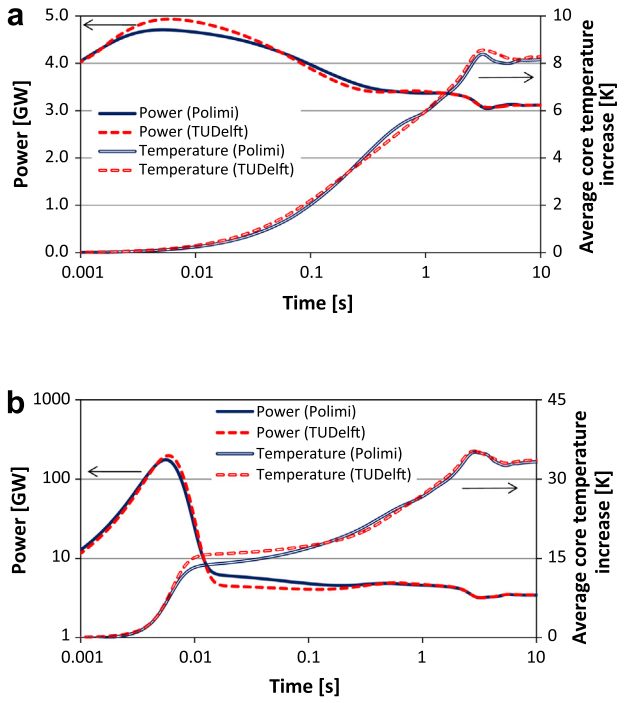

Fig. 9. Evolution of power and average temperature in the MSFR core after a step-wise reactivity insertion equal to (a) 50 pcm and (b) 200 pcm (super-prompt-critical).

Agreement between the Polimi and TUDelft models is excellent. The only visible discrepancy is in the higher power peak in the latter model, which is related to the lower feedback coefficient (Fig. 5) and β_{eff}. The higher power peak momentarily determines a higher temperature increase that, in turns, causes a steeper (and stronger) temperature decrease afterwards. However, these differences concentrate on a time-scale of 0.1–1 s, with negligible consequences on the overall energy released and therefore on the temperature increase.

6.2. Unprotected loss of flow – ULOF

A loss of flow with a complete coast-down of all the available pumps may happen in a reactor following an electricity shortage. Generally, this would compromise the heat transfer capabilities of all the loops (primary, intermediate, secondary). In the present paper, only the dynamics of the primary circuit is investigated, so that some simplifying hypotheses have to be used. In particular, it has been chosen not to vary the heat transfer capabilities at the secondary side of the heat exchanger. The underlying reason is that it is assumed that intermediate and secondary circuits in the MSFR will be designed so as to support a natural circulation regime capable to accumulate or transfer to the condenser the power produced by the reactor, at least for a few minutes.

The pumps in the primary circuit have been supposed to coast-down exponentially with a time constant of 5 s. Fig. 10 shows that the flow rate reduces rapidly during the first 20 s, after which it stabilizes thanks to the set-up of a natural circulation regime. The final flow rate is reduced by approximately 18 times compared to the initial one.

The MSFR response to the flow rate variation is shown in Fig. 11. The core average temperature initially grows as the precursor hold-back causes the power-to-flow ratio to increase. This is a well-known phenomenon in nuclear reactors and it is of great concern for classical fast reactors. For the MSFR, it appears instead as a minor problem, causing a reassuring 15 K average core temperature increase. After about 15 s the flow pattern changes in the core and the recirculation zones start to disappear. At that point, the hot salt contained in these zones flows out of the core, causing a sudden reduction of the average core temperature. After about 40 s, the mass of the hot salt originating from the recirculation zone then re-enters the core causing a small temperature increase, after which the core average temperature reduces till its asymptotic state. The power decreases monotonically and reaches in 40 s an asymptotic value equal to 500–600 MW. The power-to-flow ratio is at that point ~3–4 times higher compared to the reactor nominal conditions.

The lower flow rate reduces the out-of-core precursor decay, leading to a ~90 pcm reactivity increment that should be offset by ~15 K temperature increase. In this sense, Fig. 11 points out clearly that the core average temperature is not suitable to describe reactivity feedbacks when recirculation regions exist in the core. In fact, the core average temperature reaches an asymptotic value below the initial one. By weighting the temperature distribution with direct and adjoint fluxes provided by DALTON, the resulting effective temperature results to be increased by 13–14 K, consistently with the 90 pcm reactivity increment.

Fig. 12 shows the velocity and temperature fields for the MSFR core at the end of an ULOF. As already pointed out, the reduced flow rate eliminates the recirculation zones and the temperature monotonically increases from the bottom to the top of the core. The difference between outlet and inlet temperatures is approximately 300–400 K, consistently with the increased power-to-flow ratio. Due to the initially high core temperature caused by recirculation zones, the increased power-to-flow ratio mainly affects the outlet temperature, as the average fuel temperature must be approximately maintained to preserve the reactivity balance. In case core recirculation zones were absent in the core, the increased power-to-flow ratio would impact symmetrically inlet and outlet temperatures, except for the 13–14 K average core temperature increment. The inlet temperature would then reduce by ~150 K, causing salt freezing at the heat exchanger.

In spite of the similar predicted flow rate variation, Figs. 11 and 12 show some notable discrepancies between the Polimi and TUDelft models. Most discrepancies can be ascribed to the different prediction for the steady state temperatures (Fig. 6). In fact, when the initial flow patterns in the core disappear and the hot salt in the recirculation zone is expelled, the Polimi model predicts a stronger average core temperature decrement (Fig. 11) as a consequence of the hotter recirculation zone. In addition, core temperature variations are set by neutronic constraints, as the temperature feedback has to compensate for the reduced delayed neutron loss. As a consequence, the higher initial core temperatures in the Polimi model must be accompanied by a higher average core temperature at the new steady-state, which can only be achieved through a higher core power.

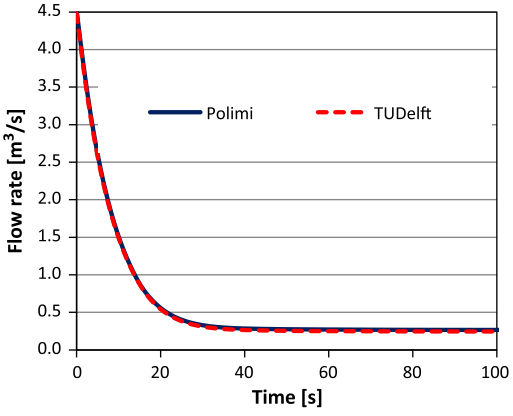

Fig. 10. Evolution of flow rate during a pump coast-down.

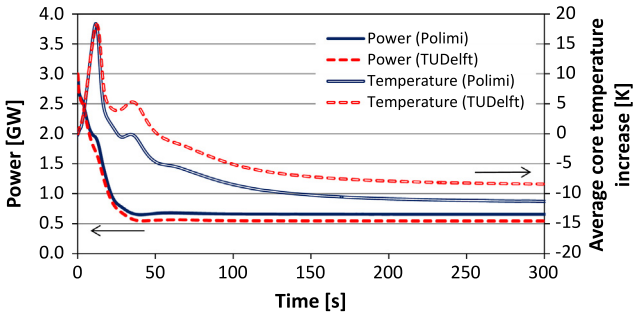

Fig. 11. Evolution of power and average temperature in the MSFR core during an ULOF.

As pointed out at the beginning of this subsection, the heat transfer capabilities at the secondary side of the heat exchanger have been maintained. A more realistic scenario would envision a reduced heat transfer coefficient and an increased temperature at the secondary side. A reduction of the cooling capabilities of the heat exchanger would clearly lead to a lower power. A complete incapability of the heat exchangers to transfer heat at the secondary side would result in a different accident, as described in the following subsection.

6.3. Unprotected loss of heat sink – ULOHS

An ULOHS will generally occur following a loss of flow at the intermediate circuit. The loss of cooling capabilities of the heat exchangers has been assumed to follow an exponential trend with a time constant of 1 s. The system response to such perturbation is reported in Fig. 13 that also shows the decay heat level.

As soon as the cooling capabilities are lost, the temperature feedbacks quickly reduce the reactor power. The precursor hold-back time maintains the reactor power above the decay heat level for about 40 s. The decay heat starts contributing substantially to the overall power generation after 20–30 s and becomes dominant after 40–50 s.

A small discrepancy is observed between Polimi and TUDelft models in terms of reactor power, which is caused by the different precursor groups considered. A more visible discrepancy is observed in the average core temperature. In fact, temperatures in the primary circuit are gradually homogenized by the disappearance of the heat source and sink. The average core temperature must converge to the average temperature in the primary loop, which in turn is set by energy conservation and is the same for the two models. Hence, the higher initial core average temperature in the Polimi model (see Section 5.1) results in a lower increment of the core average temperature. Fig. 14 shows that the predicted increment of the loop-averaged temperature is the same in the two models. It also shows the estimated increment of the loop-averaged temperature when the effect of decay heat is included, confirming its primary effect already in the first two minutes of an ULOHS.

For the MSFR, salt draining in passively cooled tanks is envisioned in case of severe accidents, with a freezing valve that is expected to open as soon as the electrical power is lost or the fuel salt heats up abnormally. Drain tanks are especially important in case of an ULOHS, as they would represent the only decay heat removal system. However, Fig. 14 shows a fuel temperature increase of 100 K in 20 s and questions the effectiveness of such system.

6.4. Chilled inlet

A reduction of the core inlet temperature will generally happen following a reduction of temperatures at the secondary circuit, which in turn may be caused e.g. by depressurization of the steam generator. The worst-case scenario is represented by a coolant temperature in the intermediate circuit that reduces to a level close to salt freezing (~723 K). This case has been considered here and it has been assumed that the salt at the secondary side of the

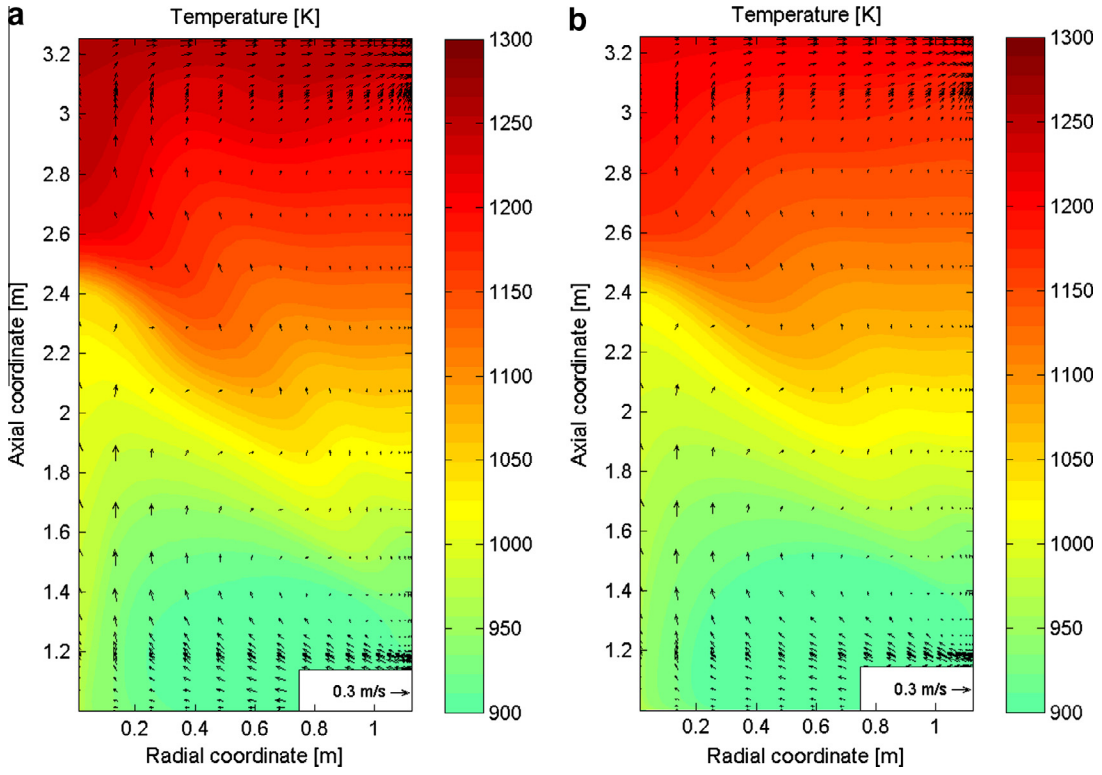

Fig. 12. Velocity and temperature fields in the core at the end of an ULOF predicted by (a) Polimi model and (b) TUDelft model.

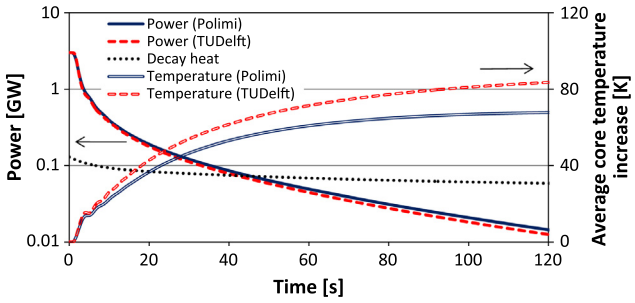

Fig. 13. Evolution of power and average temperature in the MSFR core during an ULOHS.

heat exchanger experiences a 100 K reduction governed by an exponential law with a time constant of 1 s.

The asymptotic system response to such perturbation can roughly be predicted by noticing that a reactivity balance imposes the core effective (i.e., weighted with direct and adjoint fluxes) temperature to remain unchanged at the end of the transient. In case of a simplified system without recirculation zones in the core, this would imply the average of inlet and outlet temperature to be approximately unchanged. The final reactor power would be equal to the power transferred at the heat exchangers, which in turn is roughly proportional to the difference between the average of inlet and outlet temperature and the temperature at the secondary side. In the simulated transient, such difference changes from ~150 K to ~250 K, so that the reactor power would change from 3 GW to ~5 GW. The core outlet temperature would approximately increase by half of the total increase of the inlet–outlet core temperature difference, which in turn is proportional to the power increment. In the case considered here, the outlet temperature would increase by ~30 K.

Figs. 15 and 16 plot the system response as predicted by the two developed models and the asymptotic temperature variation in the core, respectively. Following the power increment, recirculation zones tend to heat up and cause the core average temperature to increase. To preserve the effective core temperature, the average of inlet and outlet temperatures reduces at the end of the transient by −25 K and −21 K for Polimi and TUDelft models, respectively. The stronger variation in the Polimi model is related to the wider and hotter recirculation zones. A lower average of inlet and outlet temperatures implies a reduced transferred power at the heat exchanger and, consistently, a lower asymptotic core power (4.45 MW vs. 4.60 MW). The initial power peak due to the quick reduction of the inlet temperature has a limited amplitude and negligible effects on temperatures.

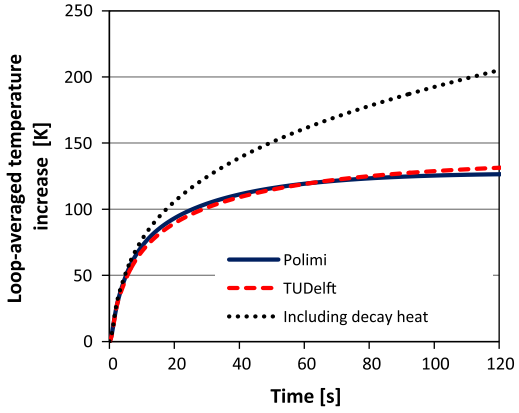

Fig. 14. Evolution of the loop-averaged temperature during an ULOHS.

The existence of recirculation zones has a beneficial effect on the core outlet temperature. As a consequence of the lower asymptotic power and of the lower average of inlet and outlet temperatures, the core outlet temperature increases by only 6 K in the TUDelft model while it remains unchanged in the Polimi model. On the other hand, when recirculation zones exist, they become the hottest regions in the core and their temperature increase can be on the order of 100 K. It is interesting to notice that a notable localized temperature increment is predicted by the Polimi model close to the lower blanket, at the flow detachment point.

As a general conclusion, a chilled-inlet accident has a mild impact on the core and only the existence of recirculation zones poses concerns in terms of temperature increase.

6.5. Pump overspeed

A pump overspeed is a kind of accident that is possible mainly in case a variable speed pump is used. An increased pump speed causes a higher delayed neutron loss, and an ensuing reactivity reduction that will be compensated by a reduction of the core temperatures. A reduced average core temperature will generally result in a lower temperature at the primary side of the heat exchanger, and, consequently, in a lower power transferred to the intermediate loop. On the other hand, a higher velocity enhances the heat transfer coefficient at the primary side, thus promoting a higher heat exchange. Finally, for a given core power and average core temperature, a higher flow rate implies a reduction of the temperature variation across the heat exchanger, which is symmetric with respect to the average temperature. This leads to an increased logarithmic average temperature at the heat exchanger. The overall result of the three mentioned effects on the asymptotic power depends on: (1) the reactivity loss due to additional delayed neutron losses; (2) the reactivity feedback coefficient associated to the salt temperature, which will determine the core temperature reduction necessary to offset the reactivity loss; and (3) the velocity dependence of the heat transfer coefficient of the heat exchanger, which will determine the enhancement in the heat transfer capabilities of the heat exchanger.

In case of the MSFR design here considered, reactivity loss is small (~3 pcm) and the very high reactivity feedback coefficient makes the reduction of core temperatures negligible. In addition, a fourth effect plays a role as a consequence of the existing recirculation zones in the core. In fact, the increased velocity increases the turbulent viscosity (and conductivity), as shown in Fig. 17. This causes the temperatures in the recirculation zones to decrease (Fig. 18), which in turn leads to higher temperatures in the flowing salt at the core centre to preserve the reactivity balance (that requires a slight reduction of the effective core temperature). Higher temperatures in the flowing salt result in higher temperatures in

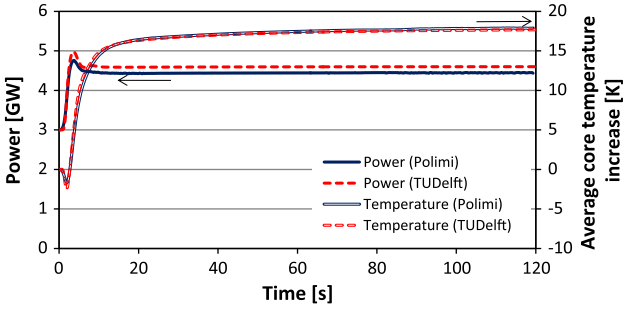

Fig. 15. Evolution of power and average temperature in the MSFR core during a chilled-inlet accident.

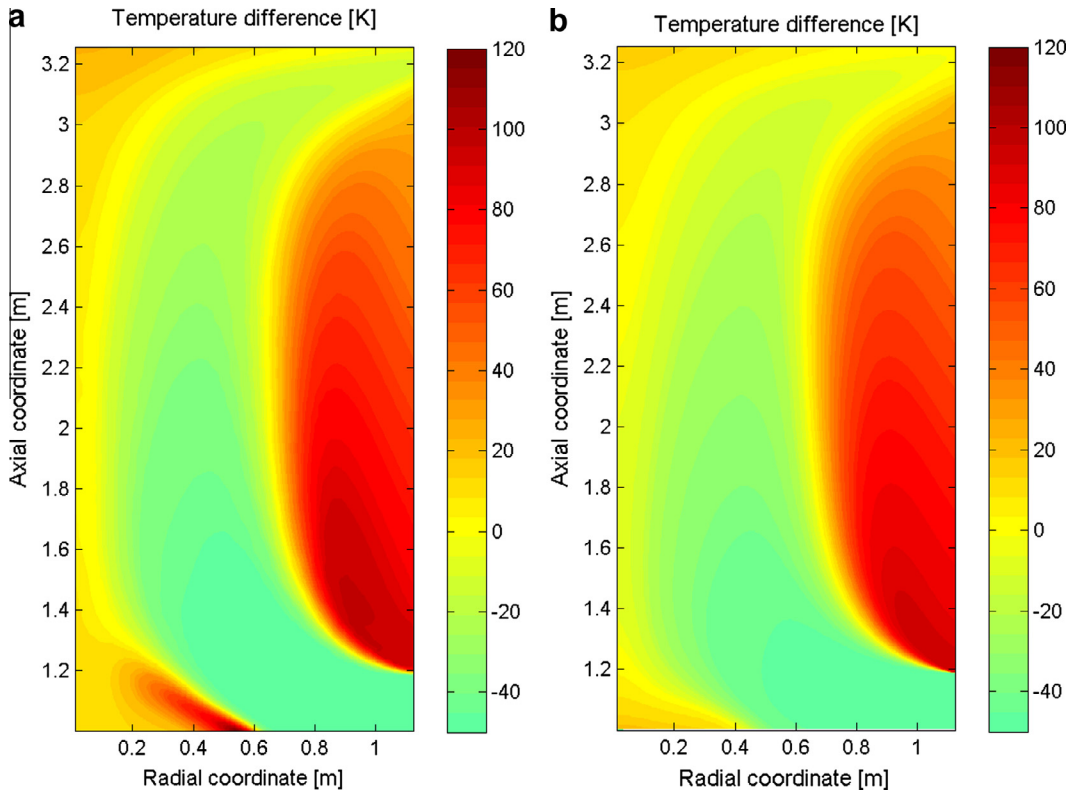

Fig. 16. Asymptotic temperature variation in case of a chilled-inlet transient predicted by (a) Polimi model and (b) TUDelft model.

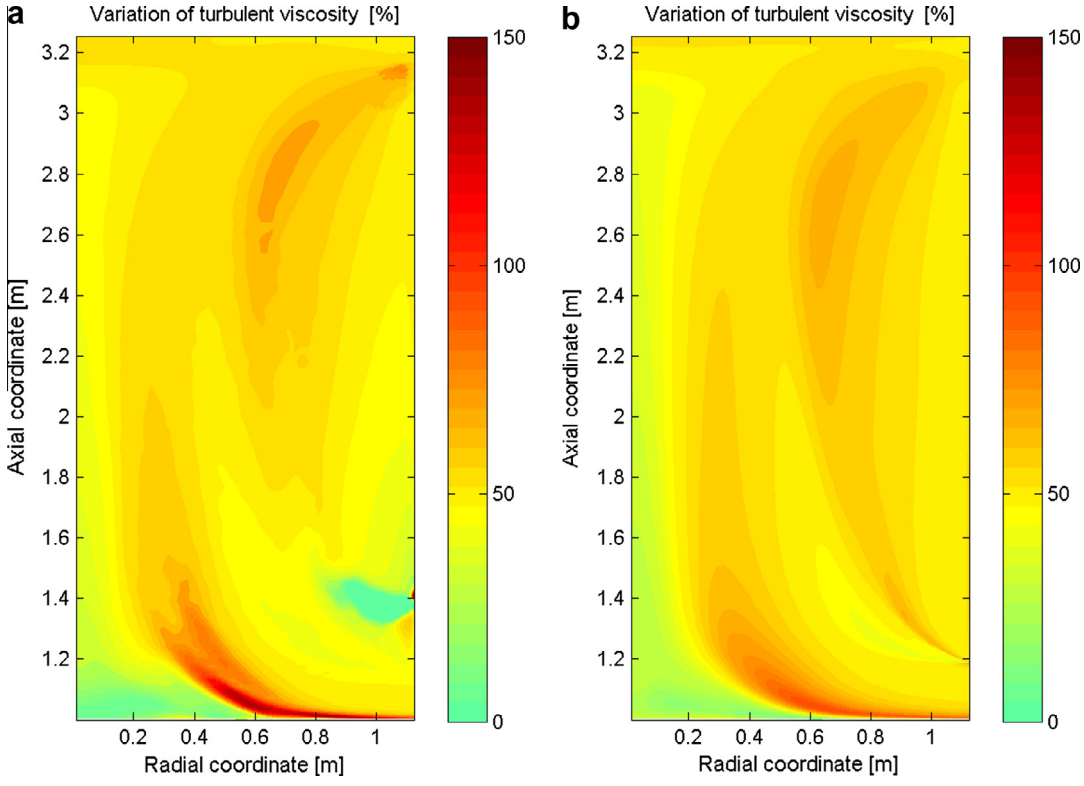

Fig. 17. Asymptotic variation of turbulent dynamic viscosity (positive numbers mean increase) in case of a pump overspeed transient predicted by (a) Polimi model and (b) TUDelft model.

the heat exchanger, which combine with the improved heat transfer coefficient and increased logarithmic temperature difference at the heat exchanger to cause a power increase, as shown in Fig. 19. The power increment predicted by the Polimi model is stronger as a consequence of the higher increment of turbulent viscosity.

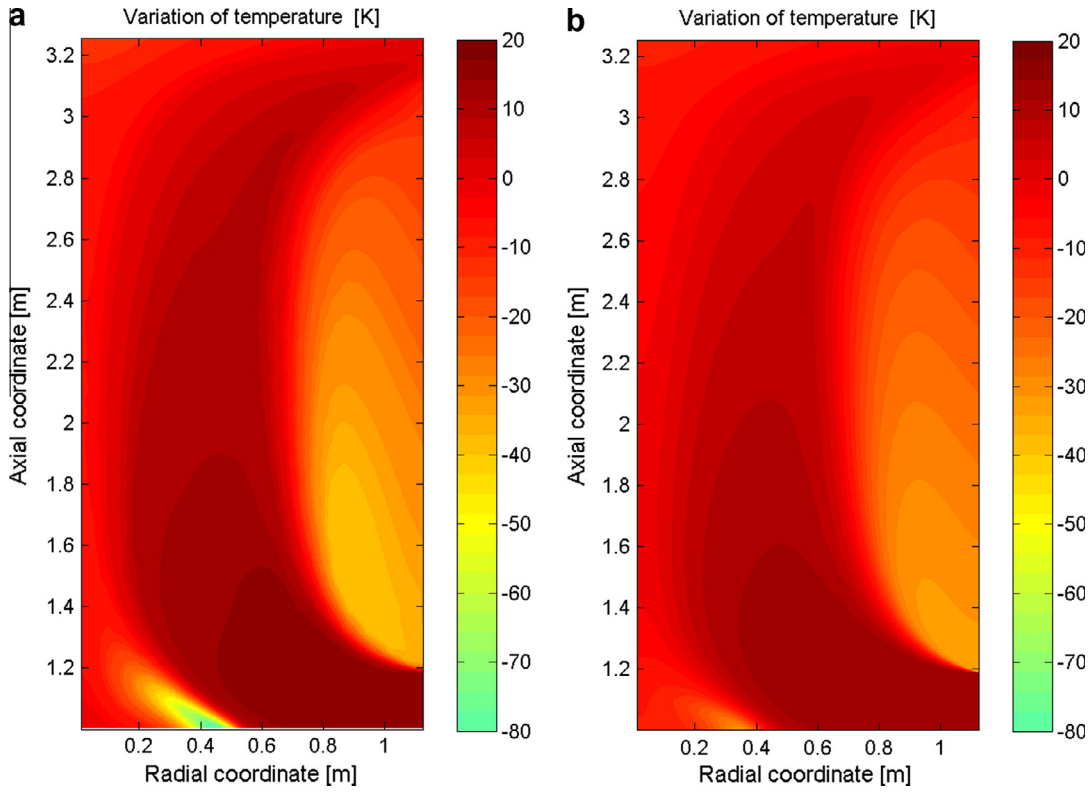

Fig. 18. Asymptotic temperature variation (positive numbers mean increase) in case of a pump overspeed transient predicted by (a) Polimi model and (b) TUDelft model.

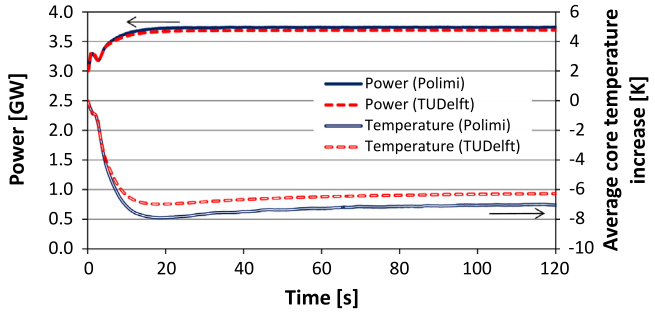

Fig. 19. Evolution of power and average temperature in the MSFR core during a pump overspeed accident.

In general, the overall effect of a pump overspeed is a reduction of the highest temperatures in the system, so that this kind of event can arguably be considered an accident (at least in the short-term).

7. Conclusions

An investigation has been carried out on the steady-state and transient behaviour of the MSFR, based on the conceptual design currently available. For this purpose, a dedicated 2-D axial-symmetric multi-physics model of the MSFR primary circuit has been developed at the Politecnico di Milano. It is capable of predicting and node-wise coupling velocity and temperature fields, neutron fluxes and precursor concentrations. The model has been systematically benchmarked with a similar model developed at the Technical University of Delft, showing a good agreement. Discrepancies have been observed in the predicted temperature field with ensuing mild impact on the transient behaviour. However, both models are suitable to obtain first important information on the MSFR steady-state and transient behaviour.

Steady-state analysis of the reactor points out some points of enhancement needed in the conceptual design. Specifically, three zones of salt recirculation have been identified in the core, causing excessive temperatures. In addition, the reduction of β_{eff} compared to a condition with static fuel has been estimated to be high, close to 60%.

The reactor response to major transient initiators has been also evaluated. Although the core design is not yet optimized, the results provide useful information on the general reactor behaviour and on the critical issues to be addressed while designing or optimizing this reactor concept. In particular, the reactor features exceptional load-following features and resistance to overpower accidents. Pump overspeed does not lead to increased core temperatures, while a chilled inlet transient may result in a notable increment of core temperatures only in case recirculation zones exist in the core. A major concern comes instead from the high specific power, leading to a quick temperature increase in case of a loss of heat sink. Natural circulation sets up in case of pump failure, but the final power-to-flow ratio is increased by 4 times and poses concerns related to both excessive outlet temperature and the possible salt freezing at the heat exchanger. However, a proper assessment would require a detailed hydrodynamic design of both the core and the out-of-core components (especially pumps and heat exchangers).

Further development of the presented models is primarily foreseen in the direction of improving the reliability of the thermal–hydraulic modelling. This would first include a better understanding of observed differences, possibly through the use of a third code. The use of turbulence models more suitable for simulating recirculation regions should also be considered (e.g., large eddy simulation). Extension of the geometrical capability of the two models to generic 2D or 3D configurations would be of great advantage to better characterize local effects, to optimize

the core design, as well as to allow the simulation of asymmetric transients like the coast-down of a single pump. Finally, in view of the unusual MSFR spectrum and fuel composition, an analysis of the uncertainty associated to nuclear data libraries should be performed.

Acknowledgements

The authors acknowledge the European Commission for funding the EVOL Project in its 7th Framework Programme. Acknowledgment is also due to all the colleagues of the participant organizations for their contributions in many different topics.

References

Benes, O., Konings, R.J.M., 2009. Thermodynamic properties and phase diagrams of fluoride salts for nuclear applications. Journal of Fluorine Chemistry 130, 22–29.

Boer, B., Lathouwers, D., Kloosterman, J.L., Van der Hagen, T.H.J.J., 2010. Validation of the DALTON-THERMIX code system with transient analyses of the HTR-10 and application to the PBMR. Nuclear Technology 170, 306–321.

Brovchenko, M., Heuer, D., Merle-Lucotte, E., Allibert, M., Capellan, N., Ghetta, V., Laureau, A., 2012. Preliminary safety calculations to improve the design of Molten Salt Fast Reactor. In: Proc. Int. Conf. PHYSOR 2012. Knoxville, Tennessee, USA, April 15–20, 2012.

Cammi, A., Di Marcello, V., Luzzi, L., Memoli, V., Ricotti, M.E., 2011. A multi-physics modelling approach to the dynamics of Molten Salt Reactors. Annals of Nuclear Energy 38, 1356–1372.

Cammi, A., Fiorina, C., Guerrieri, C., Luzzi, L., 2012. Dimensional effects in the modelling of MSR dynamics: moving on from simplified schemes of analysis to a multi-physics modelling approach. Nuclear Engineering and Design 246, 12–26.

Chadwick, M.B. et al., 2006. ENDF/B-VII.0: next generation evaluated nuclear data library for nuclear science and technology. Nuclear Data Sheets 107, 2931–3060.

Comsol, 2011. COMSOL Multiphysics® 4.2a User's Guide. COMSOL Inc.

De Zwaan, S.J., Boer, B., Lathouwers, D., 2007. Static design of a liquid-salt-cooled pebble bed reactor. Annals of Nuclear Energy 34, 83–92.

Dittus, F.W., Boelter, L.M.K., 1930. Heat transfer in automobile radiators of the tubular type. University of California Publications in Engineering 2, 443–461.

Energy from Thorium. 2013. Documents related to liquid-halide (fluoride and chloride) reactor research and development. <http://www.energyfromthorium.com/pdf/>.

EVOL, 2013. Evaluation and viability of liquid fuel fast reactor systems. <http://www.li2c.upmc.fr/>.

Fiorina, C., Aufiero, M., Cammi, A., Guerrieri, C., Krepel, J., Luzzi, L., Mikityuk, K., Ricotti, M.E., 2012. Analysis of the MSFR core neutronics adopting different neutron-transport models. In: Proc. ICONE2012 International Conference, Anaheim, California, USA, July 30 – August 3, 2012.

Fiorina, C., Aufiero, A., Cammi, A., Franceschini, F., Krepel, J., Luzzi, L., Mikityuk, K., Ricotti, M.E., 2013. Investigation of the MSFR core physics and fuel cycle characteristics. Progress in Nuclear Energy 68, 153–168.

GIF-IV, Generation IV International Forum, 2002. A Technology Road Map for Generation IV Nuclear Energy Systems. GIF-002–00, US DOE Nuclear Energy Research Advisory Committee and The Generation IV International Forum.

Incropera, F.P., DeWitt, D.P., Bergman, T.L., Lavine, A., 2006. Fundamentals of Heat and Mass Transfer. John Wiley and Sons, Hoboken, New Jersey.

Koning, A., Forrest, R., Kellett, M., Mills, R., Henriksson, H., Rugama, Y., 2006. The JEFF-3.1 nuclear data library. Nuclear Energy Agency, JEFF, Report 21.

Kophazi, J., Lathouwers, D., Kloosterman, J.L., 2009. Development of a three-dimensional time-dependent calculation scheme for molten salt reactors and validation of the measurement data of the molten salt reactor experiment. Nuclear Science and Engineering 163, 118–131.

Lathouwers, D., 2003. Iterative computation of time-eigenvalues of the neutron transport equation. Annals of Nuclear Energy 30, 1793–1806.

Leppänen, J., 2007. Development of a new Monte Carlo reactor physics code. PhD Thesis. Helsinki University of Technology.

MacPherson, H.G., 1985. The Molten Salt Reactor adventure. Nuclear Science and Engineering 90, 374380.

Merle-Lucotte, E., Heuer, D., Allibert, M., Brovchenko, M., Capellan, N., Ghetta, V., 2011. Launching the thorium fuel cycle with the Molten Salt Fast Reactor. In: Proc. Int. Conf. ICAPP 2011, Nice, France, May 2–5, 2011.

Nagy, K., Kloosterman, J.L., Lathouwers, D., Van der Hagen, T.H.J.J., 2011. New breeding gain definitions and their application to the optimization of a Molten Salt Reactor design. Annals of Nuclear Energy 38, 601–609.

Nagy, K., Kloosterman, J.L., Lathouwers, D., Van der Hagen, T.H.J.J., 2012. The effects of core zoning on the graphite lifespan and the breeding gain of a moderated molten salt reactor. Annals of Nuclear Energy 43, 19–25.

Renault, C., Delpech, M., Le Brun, C., Lecarpentier, D., Garzenne, C., Konings, R.J.M., Hosnedl, P., Matal, O., Uhlir, J., 2005. The MOST Project: Key-points and challenges for the feasibility of molten salt reactors. In: Proc. Int. Conf. ICAPP 05, Seoul, South Korea, May 15–19, 2005.

Robertson, R.C., 1971. Conceptual Design Study of a Single-Fluid Molten-Salt Breeder Reactor. Technical, Report, ORNL-4541.

SCALE: A Modular Code System for Performing Standardized Computer Analyses for Licensing Evaluations, ORNL/TM-2005/39, Version 5.1, vols. I–III. Available from Radiation Safety Information Computational Center at Oak Ridge National Laboratory as CCC-732, November 2006.

Singh, K.P., Modak, R.S., Degweker, S.B., Singh, Kanchhi, 2009. Iterative schemes for obtaining dominant alpha-modes of the neutron diffusion equation. Annals of Nuclear Energy 36, 1086–1092.

Van der Linden, B., 2012. Coupled Neutronics and Computational Fluid Dynamics for the Molten Salt Fast Reactor. MSc Thesis. Technical University of Delft, Netherlands.

Wade, D.C., Wigeland, R.A., Hill, D.J., 1997. The safety of the IFR. Progress in Nuclear Energy 31, 63–82.

Wilcox, D.C., 1998. Turbulence Modeling for CFD. DCW Industries, Inc., La Cañada, California USA.